Engineering Fracture Mechanics 78 (2011) 1478–1486

Contents lists available at ScienceDirect

Engineering Fracture Mechanics

journal homepage: www.elsevier.com/locate/engfracmech

Numerical investigation of the mode III stress intensity factors in FGMs considering the effect of graded Poisson's ratio

Rahmatollah Ghajar *, Ali Shaghaghi Moghaddam

Mechanical Properties Research Laboratory (MPRL), Dpt. of Mech. Eng., K.N. Toosi University of Technology, Pardis St., Molasdra Ave., Vanak Sq., Tehran, Iran

ARTICLE INFO

Article history:
Received 5 September 2010
Received in revised form 22 November 2010
Accepted 28 November 2010
Available online 3 December 2010

Keywords:
FGMs
Domain integral
Mode three stress intensity factor
Poisson's ratio

ABSTRACT

For cracks in functionally graded materials under pure mode three loading, this work makes use of *J*-integral in domain form to determine K_{III}. This is done as a post-processing stage in the finite element context. Numerical computations are carried out for penny-shaped and circumferential cracks. For each crack, a sensitivity analysis is done to demonstrate the trend of K_{III} with respect to the gradation indexes for modulus of elasticity and Poisson's ratio. It is realized that for a given geometry and boundary condition, K_{III} depends on gradation of both modulus of elasticity and Poisson's ratio.

1. Introduction

To assess the integrity of a cracked structure against fracture, a procedure has to be carried out to determine acceptable crack size. A crucial step in assessing the integrity of a structure is to determine the tendency to fracture. For linear elastic fracture mechanics, this is characterized by stress intensity factors [1].

Functionally graded materials (FGMs) which the distribution of two constituents, e.g. metal and ceramic, are spatially varying with space, are being considered for various applications to maximize the strength and integrity of engineering components [2]. These materials occupy a broad range of application including transport systems, biomaterials, piezoelectric and thermoelectric devices, nuclear fusion, energy conversion and cutting tools [2].

Demands for application of FGMs in modern engineering structures, necessitate the understanding of failure behavior of these materials. One of the challenging issue concerning failures of these materials is failure introduced by fracture. The fracture behavior and near tip crack fields was formerly studied by Eischen [3]. He pointed out that the same form of asymptotic crack tip fields in homogeneous materials is applicable in FGMs. In particular, the material gradation does manifest its influence in the stress intensity factors.

In literature, many numerical works analyzed two-dimensional (2D) cracks in FGMs, see for instance the following works [4–6]. The fracture behavior of 3D cracks in FGMs is still improving. Walters et al. [7] employed the *J*-integral in domain form as well as the DCT to compute the mode one stress intensity factor of semi-elliptical surface cracks in FGM plates. Yildirim et al. [8] studied the behavior of a semi-elliptical crack in a FGM coating using the DCT in conjunction with 3D finite element models. Walters et al. [9] employed the interaction energy integral to evaluate mixed mode stress intensity factors. Pure mode III stress intensity factor of a penny-shaped crack in solid cylinder under pure torsion was studied in their work. Ayhan [10,11] proposed an approach based on the use of special enriched finite elements to compute mixed-mode SIFs in 3D planar

* Corresponding author.
E-mail address: Ghajar@kntu.ac.ir (R. Ghajar).

0013-7944/$ - see front matter © 2010 Elsevier Ltd. All rights reserved.
doi:10.1016/j.engfracmech.2010.11.022

cracks in FGMs. They investigated different crack geometry imbedded in plates. Yu et al. [12] derived an interaction integral for the computation of mixed-mode SIFs in 3D nonhomogeneous materials, with continuous or discontinuous properties. Zhang et al. [13] applied a boundary-domain integral equation formulation [14,15] to analyze cracks in 3D planar crack in nonhomogeneous material.

For linear elastic materials, the *J*-integral is identical to energy release rate corresponding to the extension of crack [7]. Due to the potential source of inaccuracy for the evaluation of the crack tip contour integrals in numerical studies, the contour integral is recast into domain integral [16]. As a consequence of using domain integral, it is not required to capture precisely the details of the singular fields near the crack tip. In particular, the need to have a refined mesh near crack front and singular elements incident at crack tip are removed in this approach.

It is worth noting that in all the above mentioned works relating to 3D cracks in FGMs, for the sake of simplicity, the Poisson's ratio was kept constant. And regarding the problem geometry, merely few works studied pure mode III of fracture. Regarding the former point, it should be pointed out that for 2D cracks in FGMs, Paulino and Kim [17] demonstrated that the effect of Poisson's ratio on SIFs can be non-negligible. This is dominated by crack geometry and the scale of nonhomogeneity.

Therefore this work is aimed to explore the influence of graded elastic properties, particularly graded Poisson's ratio, on mode III of fracture in FGMs. To this aim, the domain form of *J*-integral is employed in a post-processing step in the finite element formulation. Penny-shaped and circumferential cracks under pure torsion are investigated herein to demonstrate the sensitivity of K_{III} with respect to material gradation. Numerical results are compared against the reference solutions available in literature for homogeneous and graded materials.

2. Domain integral for graded materials

According to Fig. 1a consider a generally curved planar crack. The pointwise *J*-integral at point *s* along crack front is given as [16]:

$$J(s) = \int_{\Gamma(s)} c_l H_{lj} n_j d\Gamma \tag{1}$$

where $\Gamma(s)$ refers to a contour enclosing crack tip on the plane normal to crack front at point *s*, see Fig. 1a. The components of unit normal to contour $\Gamma(s)$ is indicated by n_j and crack extension direction is denoted by c_l. The tensor H_{lj} denotes the Eshebly's energy–momentum tensor given by:

$$H_{lj} = W\delta_{lj} - \sigma_{ij}u_{i,l} \quad \text{with} \quad W = \frac{1}{2}\sigma_{mn}\varepsilon_{mn}, \quad m,n = 1,2,3 \tag{2}$$

Note that throughout the paper all the quantities are referred to the global Cartesian coordinate system.

In graded solids the *J*-integral and mode III stress intensity factor, in the absence of modes I and II, are related through the following equation [9]:

$$J(s) = \frac{1+\nu(s)}{E(s)}(K_{III})^2 \tag{3}$$

Consequently through numerical evaluation of Eq. (1), and then substituting in Eq. (3), K_{III} can be obtained. Note that $E(s)$ and $\nu(s)$ are elastic properties taken from crack front location *s*. To facilitate the numerical computation of *J*-integral, the contour integral is recast to the domain integral. To this aim, $\hat{J}(s)$ is defined as follows:

$$\hat{J}(s) = \int_{L_c}\int_{\Gamma(s)} c_l \Delta a(s) H_{lj} n_j d\Gamma ds \tag{4}$$

with L_c referring to a small length along crack front, Fig. 1b. In Eq. (4), $\Delta a(s)$ is the amplitude of the crack advance along segment L_c. Its value is set zero at each end of segment L_c and unity at point *s*. The area of integration of Eq. (4) is a tubular

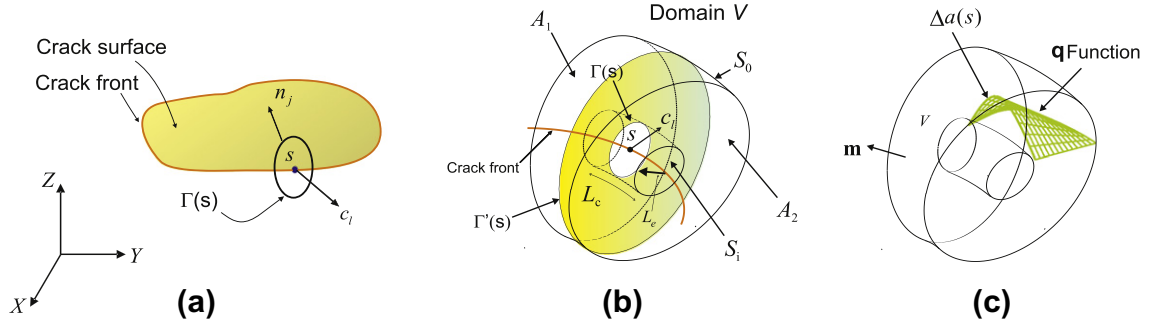

Fig. 1. (a) Planar crack with contour definition at point *s*, (b) domain representation of contour integral, (c) smooth test function within domain.

surface, S_i, obtained by sweeping contour $\Gamma(s)$ along segment L_c. Assuming L_c be small enough to neglect the variation of J-integral in this segment, Eq. (4) can be rewritten as:

$$\hat{J}(s) = J(s)\int_{L_c}\Delta a(s)ds \tag{5}$$

and then

$$J(s) = \frac{1}{\gamma}\hat{J}(s) \quad \text{with} \quad \gamma = \int_{L_c}\Delta a(s)ds \tag{6}$$

To go further with developing the domain integral, the domain of integration, V, is now defined. The domain V is obtained by sweeping contours $\Gamma(s)$ and $\Gamma'(s)$ along segment L_c, see Fig. 1b. A tubular domain is obtained where it is enclosed by inner and outer surfaces S_i and S_o and two lateral surfaces A_1 and A_2. The inner surface is characterized by L_e in which refers to the size of the smallest element incident at crack front. The size of the domain is dominated by the size of contour $\Gamma'(s)$.

Introducing a sufficiently smooth test function, **q**, within the domain V as shown in Fig. 1c:

$$q_l = \begin{cases} \Delta a(s)c_l & S_i \\ 0 & A_1, A_2, S_o \end{cases} \tag{7}$$

The Eq. (4) is rewritten as:

$$\hat{J}(s) = -\int_{S_i+S_o+A_1+A_2} q_l H_{lj} m_j dA \tag{8}$$

with m_j being the components of unit outward normal to the surface of domain V. In this work the **q** function follows the plateau variation described in [16]. Employing the divergence theorem, the integral in Eq. (8) is recast into domain form as follows:

$$\hat{J}(s) = -\int_V \left[\left(\frac{1}{2}\sigma_{mn}\varepsilon_{mn}\delta_{lj} - \sigma_{ij}u_{i,l}\right)q_{l,j} + (C_{mnpq}(X)_{,l}\varepsilon_{pq}\varepsilon_{mn})q_l\right]dV \tag{9}$$

Consequently Eq. (6) can be written as:

$$J(s) = -\frac{1}{\gamma}\int_V \left[\left(\frac{1}{2}\sigma_{mn}\varepsilon_{mn}\delta_{lj} - \sigma_{ij}u_{i,l}\right)q_{l,j} + (C_{mnpq}(X)_{,l}\varepsilon_{pq}\varepsilon_{mn})q_l\right]dV \tag{10}$$

3. Numerical computation of domain integral

In the present study, the finite element solutions for FGMs are obtained by ABAQUS through the user subroutine UMAT [18]. Herein, 20-noded brick elements with $2\times2\times2$ gauss integration points are employed. The gradation in elastic properties is modeled by selecting the material properties following the functional form at integration points.

In the finite element context, the domain V is a ring of elements, composing one or two element(s) along crack front and number of elements, depending on domain size indicated by $\Gamma'(s)$, in radial direction.

Having defined the finite domain V in the finite element context and following Gauss-quadrature rule, the integral in Eq. (10) is expressed as:

$$J(s) = \underbrace{\frac{1}{\gamma}\sum_V^{\text{elems}}\sum_p^{\text{gps}}\left[\left(\frac{1}{2}\sigma_{mn}\varepsilon_{mn}\delta_{lj} - \sigma_{ij}u_{i,l}\right)q_{l,j}\right]_p \det Jw_p}_{J^{(1)}(s)} + \underbrace{\frac{1}{\gamma}\sum_V^{\text{elems}}\sum_p^{\text{gps}}\left[(C_{mnpq}(X)_{,l}\varepsilon_{pq}\varepsilon_{mn})q_l\right]_p \det Jw_p}_{J^{(2)}(s)} \tag{11}$$

where the summation is done over eight integration points, gps, in each of elements included in domain V. Parameters w_p and det J denote the corresponding weight for integration points and determinant of the coordinate Jacobian matrix, respectively. In Eq. (11), $J^{(1)}(s)$ represents the standard form of J-integral in domain form for homogeneous materials. However, the terms $J^{(2)}(s)$ is introduced in the presence of material gradation. As a consequence of gradation in elastic properties, the derivative of material constitutive tensor, $C_{mnpq}(\mathbf{X})_{,l}$, does not vanish. For isotropic elastic FGMs, the constitutive tensor is given as [9]:

$$C_{mnpq}(\mathbf{X}) = \lambda(\mathbf{X})\delta_{mn}\delta_{pq} + \mu(\mathbf{X})(\delta_{mp}\delta_{nq} + \delta_{mq}\delta_{np}) \tag{12}$$

where δ_{mn} is the Kronecker delta, and $\mu(\mathbf{X})$ and $\lambda(\mathbf{X})$ are spatially varying Lame′ constants given as follows:

$$\begin{aligned} \lambda(\mathbf{X}) &= \frac{E(\mathbf{X})\nu(\mathbf{X})}{(1+\nu(\mathbf{X}))(1-2\nu(\mathbf{X}))} \\ \mu(\mathbf{X}) &= \frac{E(\mathbf{X})}{2(1+\nu(\mathbf{X}))} \end{aligned} \tag{13}$$

$E(\mathbf{X})$ and $v(\mathbf{X})$ are varying elastic properties. In Cartesian coordinate system the derivative of the constitutive tensor is given as:

$$\frac{\partial C_{mnpq}(\mathbf{X})}{\partial X_l} = \frac{\partial C_{mnpq}(\mathbf{X})}{\partial E(\mathbf{X})}\frac{\partial E(\mathbf{X})}{\partial X_l} + \frac{\partial C_{mnpq}(\mathbf{X})}{\partial v(\mathbf{X})}\frac{\partial v(\mathbf{X})}{\partial X_l} \tag{14}$$

where

$$\begin{aligned}\frac{\partial C_{mnpq}(\mathbf{X})}{\partial E(\mathbf{X})} &= \frac{1}{E(X)}C_{mnpq}(\mathbf{X})\\ \frac{\partial C_{mnpq}(\mathbf{X})}{\partial v(\mathbf{X})} &= \frac{E(\mathbf{X})(1+2v(\mathbf{X})^2)}{[(1+v(\mathbf{X}))(1-2v(\mathbf{X}))]^2}\delta_{mn}\delta_{pq} - \frac{E(\mathbf{X})}{2(1+v(\mathbf{X}))^2}(\delta_{mp}\delta_{nq}+\delta_{mq}\delta_{np})\end{aligned} \tag{15}$$

In the finite element formulation, the derivatives of material properties at integration points are computed using isoparametric interpolations [19]:

$$\begin{aligned}\frac{\partial E(\mathbf{X})}{\partial X_l} &= \sum_{I=1}^{20} E_I \frac{\partial N_I}{\partial X_l},\\ \frac{\partial v(\mathbf{X})}{\partial X_l} &= \sum_{I=1}^{20} v_I \frac{\partial N_I}{\partial X_l}\end{aligned} \tag{16}$$

where E_I and v_I are nodal values of modulus of elasticity and Poisson's ratio, respectively, and N_I are shape functions.

4. Numerical examples

4.1. Penny-shaped crack in a solid cylinder

In this example a penny-shaped crack embedded in a solid cylinder subjected to pure torsion is studied. The geometry is characterized as $R/r_c = 5$, $H/R = 3$, $r_c = 20$ where r_c, R and H refer to crack radius, cylinder radius and cylinder height, respectively, see Fig. 2a. The finite element mesh employed here, comprises 11,384 elements and 48,662 nodes. The size of the smallest element incident at crack front is $L_e = 0.4$, see Fig. 2b.

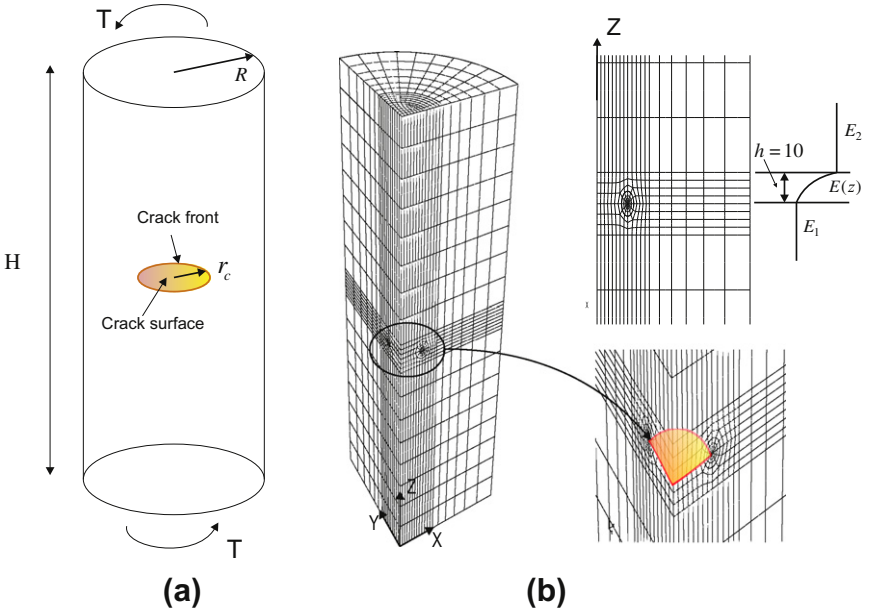

Fig. 2. (a) Characteristic geometrical features of the penny-shaped crack, (b) corresponding finite element mesh for a quarter of the model developed in ABAQUS.

Now let modulus of elasticity vary in axial direction as:

$$E(z)=\begin{cases} E_1 & z<\frac{H}{2} \\ E_1 e^{\beta'\left(z-\frac{H}{2}\right)} & \frac{H}{2}\leqslant z\leqslant \frac{H}{2}+h \\ E_2 & Z>\frac{H}{2}+h \end{cases}, \quad \text{with} \quad \beta'=\frac{1}{h}\ln\left(\frac{E_2}{E_1}\right) \tag{17}$$

where β' is the gradation index for modulus of elasticity. This variation is shown in Fig. 2b. Walters et al. [9] and Ozturk and Erdogan [20] studied this crack, in particular for graded modulus of elasticity following Eq. (17) and constant Poisson's ratio, $v = 0.3$. They reported normalized mode III stress intensity factors, K_{IIIN}, as:

$$K_{IIIN}=\frac{K_{III}}{\tau_o\sqrt{\pi r_c}} \tag{18}$$

where T_o is the magnitude of crack face traction [9]. For the sake of comparison, results obtained from the present approach are compared to the available results in literature assuming the same functional form employed in the references. The results are tabulated in Table 1. From Table 1, it is obvious that the results obtained from the present approach match closely to those of analytical solution [20].

As an alternative, the influence of material gradation in radial direction is now studied. The elastic properties are assumed to vary according to the following form:

$$\begin{aligned} &E(r)=E_o e^{\beta r}, \quad v(r)=v_o e^{\eta r} \\ &with \beta=\frac{1}{R}\ln\left(\frac{E_R}{E_o}\right), \quad \eta=\frac{1}{R}\ln\left(\frac{v_R}{v_o}\right) \end{aligned} \tag{19}$$

In Eq. (19) E_R and v_R represent material properties at $r = R$, where E_o and v_o represent material properties at $r = 0$. Now a sensitivity analysis is carried out to demonstrate the trend of K_{IIIN} with respect to β and η. This is shown in Table 2. For better clarity of the effect of Poisson's ratio gradation on SIF, the percentage change in SIF due to change in η for a given β is also shown in parenthesis in the relevant tables. It is observed that K_{IIIN} depends on gradation of both modulus of elasticity and Poisson's ratio. On the other hand, it is obvious that the influence of gradation of Poisson's ratio is considerable. For instance for $\beta = 0.03$, difference between K_{IIIN} for $\eta = 0.015$ and $\eta = 0$ is 21%. In this example for a given β, K_{IIIN} increases by increasing η. However, for a given η, K_{IIIN} decreases by increasing β.

4.2. External circumferential crack in a hollow cylinder

According to Fig. 3a consider an external circumferential crack in a hollow cylinder subjected to pure torsion. The geometry is characterized by inner radius $r_i = 1$, outer radius $r_o = 2$ and height $H = 16$. In the present work two crack geometries are

Table 1
Normalized stress intensity factor for a Penny-shaped crack in a solid cylinder under Torsion.

E_2/E_1	Results	K_{IIIN}	% difference
1	Ozturk and Erdogan [18]	0.424	–
	Walters et al. [9]	0.427	0.71
	Present	0.425	0.24
0.1	Ozturk and Erdogan [18]	0.509	–
	Walters et al. [9]	0.510	0.20
	Present	0.508	−0.20
3	Ozturk and Erdogan [18]	0.395	–
	Walters et al. [9]	0.398	0.76
	Present	0.396	0.25

Table 2
Sensitivity of K_{IIIN} to gradation indexes β and η for the penny-shaped crack in a solid cylinder. (The percentage change in SIF due to change in η for a given β is shown in parenthesis).

η	β						
	0.030	0.023	0.016	0.000	−0.016	−0.023	−0.030
0.015	0.0722 (21.1)	0.1149 (20.6)	0.1813 (19.9)	0.5026 (18.4)	1.2991 (16.4)	1.9048 (15.5)	2.7429 (14.5)
0.004	0.063 (5.7)	0.1006 (5.6)	0.1594 (5.4)	0.4463 (5.1)	1.1681 (14.7)	1.7231 (4.5)	2.4974 (4.2)
0.001	0.0603 (1.2)	0.0964 (1.2)	0.1528 (1.1)	0.429 (1.1)	1.1265 (1)	1.6645 (0.9)	2.4168 (0.9)
0.000	0.060	0.095	0.151	0.425	1.116	1.649	2.396
−0.001	0.059 (−1)	0.0943 (−1)	0.1495 (−1.1)	0.4202 (−1)	1.1052 (−0.9)	1.6344 (−0.9)	2.3752 (−0.9)
−0.004	0.0565 (−5.2)	0.0904 (−5.1)	0.1435 (−5.1)	0.404 (−4.8)	1.0654 (−4.5)	1.5777 (−4.3)	2.2963 (−4.2)
−0.015	0.0499 (−16.3)	0.08 (−16.1)	0.1271 (−15.9)	0.3594 (−15.3)	0.9533 (−14.6)	1.4162 (−14.1)	2.0686 (−13.7)

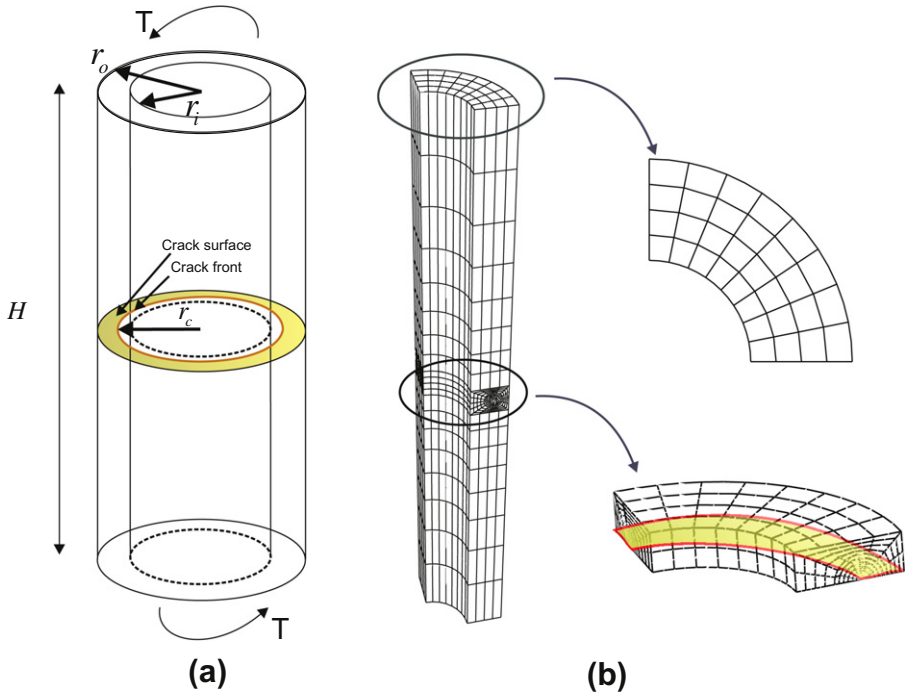

Fig. 3. (a) Characteristic geometrical features of the external circumferential crack in a hollow cylinder, (b) corresponding finite element mesh for a quarter of the model developed in ABAQUS.

considered as $r_c = 1.2$ and $r_c = 1.6$, with r_c being the crack radius. The finite element mesh for crack with $r_c = 1.2$ comprises 8704 elements and 37,664 nodes while for crack with $r_c = 1.6$ comprises 7168 elements and 30,944 nodes. The size of the smallest element incident at crack front is $L_e = 0.02$, see Fig. 3b.

Kazuyoshi et al. [21] studied this crack analytically in homogeneous material. For the sake of comparison, the solution for K_{III} for elastic properties taken as $E = 1$ and $\nu = 0.1$ is tabulated in Table 3. It is inferred that a good agreement with reference to analytical solution is obtained.

Now let us consider elastic properties varying in radial direction through an exponential form as:

$$E(r) = E_i e^{\beta(r-r_i)}, \quad \nu(r) = \nu_i e^{\eta(r-r_i)} \quad \text{with} \quad \beta = \frac{1}{r_o - r_i} \ln\left(\frac{E_o}{E_i}\right), \quad \eta = \frac{1}{r_o - r_i} \ln\left(\frac{\nu_o}{\nu_i}\right) \tag{20}$$

where β and η are gradation indexes for elastic properties. In Eq. (20) subscripts i and o denote elastic properties taken from inner and outer radii, respectively. A sensitivity analysis of K_{III} with respect to gradation indexes are shown in Tables 4 and 5 for $r_c = 1.2$ and $r_c = 1.6$, respectively.

From Tables 4 and 5, it is inferred that both gradation indexes do affect K_{III}, However the sensitivity to β is superior. It should be pointed out that for a given β, K_{III} decreases by increasing η. However, for a given β, K_{III} increases by increasing β.

4.3. External circumferential crack in a solid cylinder

In this example an external circumferential crack in a solid cylinder is investigated, see Fig. 4a. The geometry is described by height $H = 50$, radius $R = 10$ and crack length $a = 1$. The finite element mesh, composing 2592 elements, 16,497 nodes and the size of the smallest element incident at crack front as $L_e = 0.1$ is shown in Fig. 4b. The analytical solution for this crack geometry in homogeneous material is provided in [22].

Numerical solution for K_{III} extracted from J-integral for this crack geometry is 0.122 while the analytical solution is 0.123 [22], with elastic properties taken as $E = 1$ and $\nu = 0.1$. Now an exponential variation of elastic properties similar to the one in

Table 3
The solution for K_{III} in homogeneous material for external circumferential crack in a hollow cylinder.

r_c	Li and Zou [19]	Present	% Difference
1.2	0.341	0.337	−1.2
1.6	0.124	0.123	−0.8

Table 4
Sensitivity of K_{III} to gradation indexes β and η for the external circumferential crack in a hollow cylinder, $r_c = 1.2$. (The percentage change in SIF due to change in η for a given β is shown in parenthesis).

η	β				
	2.303	1.099	0.000	−1.099	−2.303
1.386	0.381 (−0.8)	0.357 (−0.8)	0.333 (−1.2)	0.308 (−1.2)	0.278 (−1.8)
0.406	0.383 (−0.3)	0.359 (−0.3)	0.335 (−0.6)	0.31 (−0.6)	0.281 (−0.7)
0.000	0.384	0.360	0.337	0.312	0.283
−0.406	0.386 (0.5)	0.362 (0.6)	0.339 (0.6)	0.314 (0.6)	0.285 (0.7)
−1.386	0.39 (1.6)	0.367 (1.9)	0.344 (2.1)	0.319 (2.2)	0.29 (2.5)

Table 5
Sensitivity of K_{III} to gradation indexes β and η for the external circumferential crack in hollow cylinder, $r_c = 1.6$. (The percentage change in SIF due to change in η for a given β is shown in parenthesis).

η	β				
	2.3026	1.0986	0.0000	−1.0986	−2.3026
1.3863	0.167 (−2.3)	0.142 (−3.4)	0.117 (−4.9)	0.092 (−5.2)	0.066 (−7)
0.4055	0.17 (−0.6)	0.145 (−1.4)	0.121 (−1.6)	0.095 (−2.1)	0.069 (−2.8)
0.0000	0.171	0.147	0.123	0.097	0.071
−0.4055	0.173 (1.2)	0.149 (1.4)	0.124 (0.8)	0.099 (2.1)	0.072 (1.4)
−1.3863	0.176 (2.9)	0.152 (3.4)	0.128 (4.1)	0.103 (6.2)	0.076 (7)

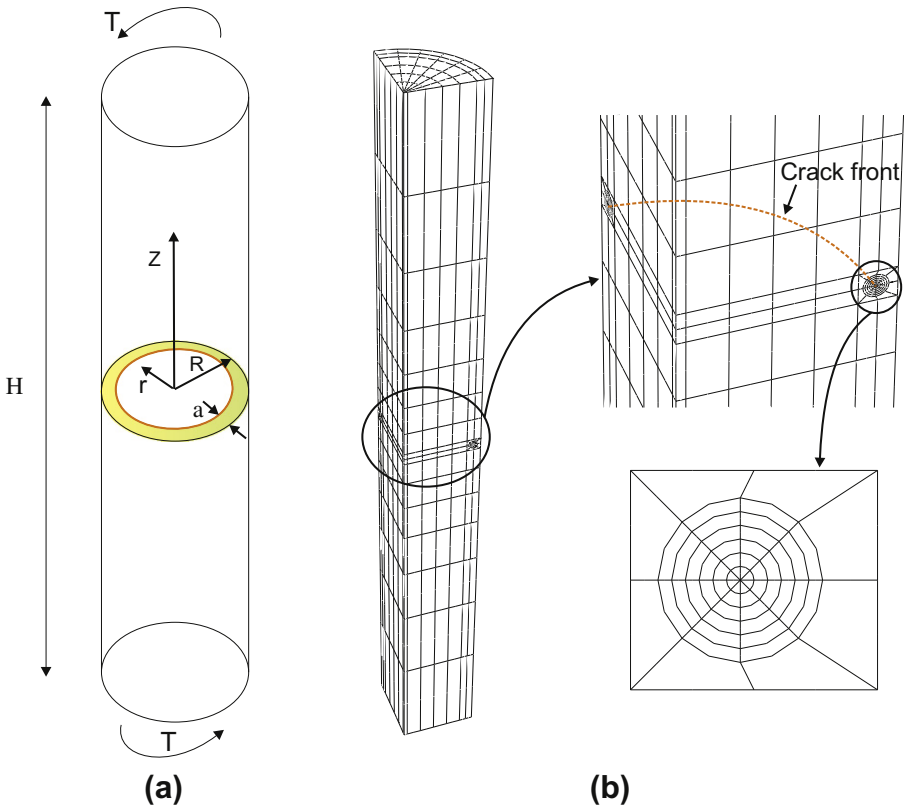

Fig. 4. (a) Characteristic geometrical features of the external circumferential crack in a solid cylinder, (b) corresponding finite element mesh for a quarter of the model developed in ABAQUS.

Eq. (19) is considered herein. The results for K_{III} with respect to different gradation indexes is shown in Table 6. It is inferred that the dependency of K_{III} to β is superior to that of η.

In this example it is of interest to examine the domain independency of J-integral. To this aim, the J-integral and its components, introduced in Eq. (11), are evaluated for different domains and different scale of nonhomogeneity. This is shown in

Table 6
Sensitivity of K_{III} to gradation indexes β and η for the external circumferential crack in solid cylinder. (The percentage change in SIF due to change in η for a given β is shown in parenthesis).

η	β						
	0.340	0.230	0.161	0.000	−0.161	−0.230	−0.340
0.1386	0.178 (−2.7)	0.159 (−3.0)	0.146 (−3.9)	0.116 (−4.9)	0.086 (−6.5)	0.074 (−7.5)	0.056 (−8.2)
0.0405	0.182 (−0.5)	0.163 (−0.6)	0.15 (−1.3)	0.12 (−1.6)	0.091 (−1.1)	0.078 (−2.5)	0.06 (−1.6)
0	0.183	0.164	0.152	0.122	0.092	0.080	0.061
−0.0405	0.185 (1.1)	0.166 (1.2)	0.153 (0.7)	0.123 (0.8)	0.093 (1.1)	0.081 (1.3)	0.062 (1.6)
−0.1386	0.186 (1.6)	0.167 (1.8)	0.155 (2)	0.125 (2.5)	0.095 (3.3)	0.083 (3.8)	0.064 (4.9)

Table 7
Contribution of terms in *J*-integral for different domain sizes and scale of nonhomogeneities.

Material gradation	Contribution	Domain#1	Domain#2	Domain#3	Domain#4
$E_2/E_1 = 1$	$J^{(1)}(s)$	16.3077	16.3303	16.3311	16.3327
$\nu_2/\nu_1 = 1$	$J^{(2)}(s)$	0.0000	0.0000	0.0000	0.0000
$\nu_1 = 0.1$	$J(s)$	16.3077	16.3303	16.3311	16.3327
$E_2/E_1 = 30$	$J^{(1)}(s)$	1.7071	1.6532	1.6008	1.5510
$\nu_2/\nu_1 = 1$	$J^{(2)}(s)$	0.0300	0.0866	0.1391	0.1892
$\nu_1 = 0.1$	$J(s)$	1.7371	1.7398	1.7399	1.7402
$E_2/E_1 = 30$	$J^{(1)}(s)$	1.9688	1.9136	1.8592	1.8072
$\nu_2/\nu_1 = 4$	$J^{(2)}(s)$	0.0310	0.0895	0.1441	0.1964
$\nu_1 = 0.1$	$J(s)$	1.9997	2.0031	2.0033	2.0036
$E_2/E_1 = 1/30$	$J^{(1)}(s)$	91.6840	95.3495	98.9385	102.6757
$\nu_2/\nu_1 = 0.25$	$J^{(2)}(s)$	−1.7714	−5.3065	−8.8878	−12.6114
$\nu_1 = 0.4$	$J(s)$	89.9126	90.0430	90.0506	90.0643

Table 7. It is concluded that, in the presence of gradation in elastic properties, the term $J^{(2)}(s)$ should be included to assure the domain independency of the results. And the contribution of $J^{(2)}(s)$ is superior when the material gradation increases. It is clear that despite existing material nonhomogeneity, the *J*-integral is domain independent.

5. Conclusion

In the present work, the mode III stress intensity factor in FGMs considering gradation on elastic properties has been numerically investigated. To this aim the *J*-integral in domain form was employed, in particular it was modified to account for gradation of Poisson's ratio. To assess the accuracy of the present numerical scheme, benchmark solutions from literature available for homogeneous material and FGMs were studied. It was observed that accurate results are obtained compared to the reference solutions. Further, to investigate the influence of elastic properties on the mode III SIF, different scale of gradation for both modulus of elasticity and Poisson's ratio were considered. It was observed that generally gradation of modulus of elasticity has more influence on K_{III}. However its influence is altered for different crack geometries and gradation index η. Percentage change in K_{III} due to change in η for a given β were drawn in relevant tables for better clarity of the effect of gradation of Poisson's ratio. It was concluded that the influence of gradation of Poisson's ratio can be non-negligible and has to be taken into account, e.g. penny-shaped crack in a solid cylinder. Percentage change in K_{III} depends on the crack geometry and gradation indexes η and β. Generally, it is inferred that accurate estimation of mode III SIF requires a numerical scheme to account for gradation of modulus of elasticity and Poisson's ratio, as well. Domain integral formulation, including the term to reflect the influence of material gradation, showed to yield accurate and domain independent results. With the help of domain integral, the need to have refined mesh near crack front is removed. As a consequence, accurate results are obtained despite using coarser mesh.

References

[1] Anderson TL. Fracture mechanics-fundamentals and applications. 2nd ed. Boca Raton, FL: CRC Press; 1995.
[2] Birman V, Byrd LW. Modeling and analysis of functionally graded materials and structures. Appl Mech Rev 2007;60:195–216.
[3] Eischen J. Fracture of nonhomogeneous materials. Int J Fract 1983;34:3–22.
[4] Dolbow JE, Gosz M. On the computation of mixed-mode stress intensity factors in functionally graded materials. Int J Solids Struct 2002;39:2557–74.
[5] Rousseau C, Tippur HV. Evaluation of crack tip fields and stress intensity factors in functionally graded elastic materials: cracks parallel to elastic gradient. Int J Fract 2002;114:87–111.
[6] Kim J, Paulino GH. Finite element evaluation of mixed mode stress intensity factors in functionally graded materials. Int J Numer Meth Eng 2002;53:1903–35.
[7] Walters MC, Paulino GH, Dodds RH. Stress-intensity factors for surface cracks in functionally graded materials under mode-I thermomechanical loading. Int J Solids Struct 2004;41:1081–118.
[8] Yildirim B, Dag S, Erdogan F. Three dimensional fracture analysis of FGM coatings under thermomechanical loading. Int J Fract 2005;132:369–95.

[9] Walters MC, Paulino GH, Dodds RH. Computation of mixed-mode stress intensity factors for cracks in three-dimensional functionally graded solids. J Eng Mech 2006;132:1–15.
[10] Ayhan AO. Stress intensity factors for three-dimensional cracks in functionally graded materials using enriched finite elements. Int J Solids Struct 2007;44:8579–99.
[11] Ayhan AO. Three-dimensional mixed-mode stress intensity factors for cracks in functionally graded materials using enriched finite elements. Int J Solids Struct 2009;46:796–810.
[12] Yu H, Wu L, Guo L, Wu H, Du S. An interaction integral method for 3D curved cracks in nonhomogeneous materials with complex interfaces. Int J Solids Struct 2010;47:2178–89.
[13] Zhang C, Cui M, Wang J, Gao XW, Sladek J, Sladek V. 3D crack analysis in functionally graded materials. Eng Fract Mech 2010;78:585–604.
[14] Chen JT, Hong H-K. Review of dual boundary element methods with emphasis on hypersingular integrals and divergent series. Appl Mech Rev, ASME 1999;52:17–33.
[15] Hong H-K, Chen JT. Derivations of integral equations of elasticity. J Eng Mech, ASCE 1988;114:1028–44.
[16] Shih CF, Moran B, Nakamura T. Energy release rate along a three-dimensional crack front in a thermally stressed body. Int J Fract 1986;30:79–102.
[17] Paulino GH, Kim J. On the Poisson's ratio effect on mixed-mode stress intensity factors and T-stress in functionally graded materials. Int J Comput Eng Sci 2004;5:833–61.
[18] Hibbitt, Karlsson, Sorensen, Inc. ABAQUS/standard users manual, v. 6.7. Pawtucket, Rhode Island; 2006.
[19] Li C, Zou Z. Stress intensity factors for a functionally graded material cylinder with an external circumferential crack. Fatigue Fract Eng M 1998;21:1447–57.
[20] Ozturk M, Erdogan F. Axisymmetric crack problem in bonded materials with a graded interfacial region. Int J Solids Struct 1996;33:193–219.
[21] Kazuyoshi S, Toshikazu S, Takashi K. The torsion of an infinite hollow cylinder with an external crack. Int J Eng Sci 1978;16:707–15.
[22] Malits P. Torsion of a cylinder with a shallow external crack. Int J Solids Struct 2009;46:3061–7.